JTTEE5 22:1170–1183
DOI: 10.1007/s11666-013-9970-3
1059-9630/$19.00 © ASM International

Thermal Spray Maps: Material Genomics of Processing Technologies

Andrew Siao Ming Ang, Noppakun Sanpo, Mitchell L. Sesso, Sun Yung Kim, and Christopher C. Berndt

(Submitted January 31, 2013; in revised form June 16, 2013)

There is currently no method whereby material properties of thermal spray coatings may be predicted from fundamental processing inputs such as temperature-velocity correlations. The first step in such an important understanding would involve establishing a foundation that consolidates the thermal spray literature so that known relationships could be documented and any trends identified. This paper presents a method to classify and reorder thermal spray data so that relationships and correlations between competing processes and materials can be identified. Extensive data mining of published experimental work was performed to create thermal spray property-performance maps, known as "TS maps" in this work. Six TS maps will be presented. The maps are based on coating characteristics of major importance; i.e., porosity, microhardness, adhesion strength, and the elastic modulus of thermal spray coatings.

Keywords adhesion, data mining, elastic modulus, genomic analysis, hardness, property map, sliding wear, spray parameters, thermal spray

1. Introduction

In the field of surface engineering, thermal spray is a generic term for a group of processes in which liquid droplets, semi-molten or solid particles impact and are then deposited onto a substrate as morphological features that are known as "splats" (Ref 1). A coating can be generated if the accelerated droplets or particles can (i) plastically deform or rapidly cool into thin lamellae on impact, (ii) adhere to the surface, and (iii) overlap and interlock into a consolidated coating during the solidification process. The coating is usually generated in multiple passes from 5 to 100 depending on the thickness required. The coating material may be metal based, a ceramic oxide or carbide, a polymer, or a composite; all of which may be in the morphology of a powder, wire, or rod (Ref 2).

There are two important variables for any thermal spray process, flame jet temperature and particle velocity, which together are known as "TV relationships" (Ref 3, 4). This refers to the direct spatial interaction of three physical distributions, i.e., the feedstock characteristics, the high energy temperature field, and the gas jet velocity field, that influence directly the spreading of the molten particle during splat formation. The splats or solidified molten particles, along with other important artifacts such as oxides, voids, and cracks, are the fundamental building blocks of a thermal spray coating.

Andrew Siao Ming Ang, Noppakun Sanpo, Mitchell L. Sesso, SunYung Kim, and **Christopher C. Berndt**, Industrial Research Institute Swinburne, Swinburne University of Technology, H66, P.O. Box 218, Hawthorn, VIC 3122 , Australia; **Andrew Siao Ming Ang, Noppakun Sanpo, Mitchell L. Sesso,** and **Christopher C. Berndt**, Defence Materials Technology Centre (DMTC), Swinburne University of Technology, P.O. Box 218, Hawthorn VIC 3122, Australia; and **Christopher C. Berndt**, Department of Materials Science and Engineering, Stony Brook University, Stony Brook, NY 11794. Contact e-mail: aang@swin.edu.au.

Abbreviations

APS	Atmospheric plasma spray
ASTM	American Society for Testing and Materials
CAPS	Controlled atmosphere plasma spray
CS	Cold spray
D-Gun®	Detonation gun spray
FS	Flame spray
HA	Hydroxapapite
HRC	Rockwell hardness C-scale
HVOF	High-velocity oxygen fuel spray
HVSFS	High-velocity suspension flame spray
LPPS	Low pressure plasma spray
PTWA	Plasma-transferred wire arc spray
RF	Radio frequency
SOD	Standoff distance
SPS	Suspension plasma spray
SPPS	Solution precursor plasma spray
TAT	Tensile adhesion test
TBC	Thermal barrier coating
TS	Thermal spray
TV	Flame temperature and particle velocity
TWA	Twin Wire Arc
VPS	Vacuum plasma spray
WC	Tungsten monocarbide
WC-Co	Tungsten carbide-cobalt
WSP	Water-stabilized plasma spray
YSZ	Yttria-stabilized zirconia

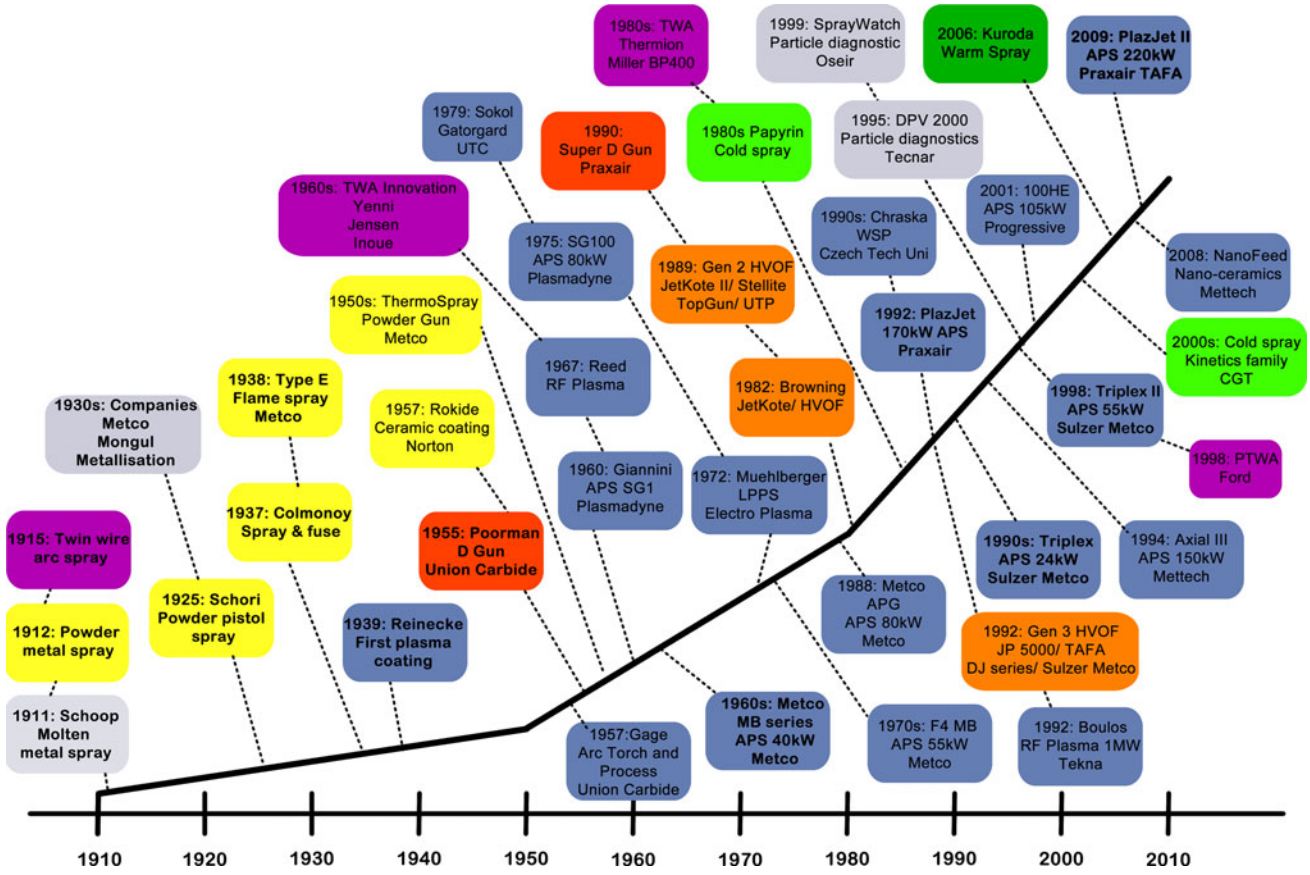

Fig. 1 Timeline of thermal spray processes

Therefore, it follows that the final coating microstructure and its properties are influenced by the feedstocks and thermal spray processes employed. In other words, TV relationships translate into functional properties that are necessary for specific applications.

A large number of factors, such as spray parameters and spray materials, influence the TV value (Ref 5, 6). Thus, under practical operational procedures, it is notionally assumed that the thermal spray operator has optimized heating and acceleration of particles to achieve the favored microstructure that is purposely designed for the intended application. The combination of material selection, coating process, and coating conditions influences the final coating microstructure and, hence, the desired properties. This challenge has existed since the invention of thermal spray in the early 1900s (Ref 7) and has resulted in several evolution cycles for the field of thermal spray. The timeline for key developments of thermal spray processes is presented in Fig. 1, with the accompanying references found in Table 1.

Although there is a vast amount of literature documenting the development of new coating materials or processes, the thermal spray field lacks a systematic method that integrates materials' chemistry, processing, structure, property, and performance. On the other hand, there has been a paradigm shift in materials research and development from an experimental knowledge base toward a material genomic approach (Ref 8, 9).

The current work is founded on a material genomic approach and bridges the materials science and engineering goals for thermal spray technology by undertaking a survey of the available literature. Property cross-plots, as first proposed by Ashby (Ref 10), are created and used to quantify property-performance relations in a broad methodology for materials selection.

2. Thermal Spray Technology

The thermal spray processes can be classified into three broad families (Ref 2, 11): (i) the use of combustion heat sources, namely, the flame, detonation gun, and HVOF processes; (ii) another family of processes using electrical energy, either in the form of plasma or as an arc, and (iii) the third being a recent extension to the thermal spray family (Ref 12) known as cold spray (CS), kinetic spray, or hypersonic spray, which uses the energy that evolves from an expanding gas.

Another way to understand thermal spray processes is by mapping the coating formation process that influenced the particle temperature and velocity, Fig. 2. Along with Table 2, which was compiled from references (Ref 1, 2),

Table 1 List of references for timeline of TS development (as shown in Fig. 1)

Year	Application	Lead inventor/Company	Reference details
1911	Flame spray	M.U. Schoop	M.U. Schoop, "Improvements in or connected with the coating of surfaces with metal, applicable also for Soldering or Uniting Metals and other Materials." United Kingdom Patent No. A.D 5,712 U. K. P. Office, 1911
1912	Flame spray	M.U. Schoop	M.U. Schoop, "An Improved Process of Applying Deposits of Metal or Metallic Compounds to Surfaces." United Kingdom Patent No. A.D.21066. U. K. P. Office, 1912
1915	Electric wire arc spray	M.U. Schoop	M.U. Schoop, "Apparatus for Spraying Molten Metal and Other Fusible Substances." USA Patent No. 1,133,507. U. S. P. Office, 1915
1925	Flame spray/Pistol	F. Schori,	F. Schori, "Improved Process of and Apparatus for Atomizing." United Kingdom Patent No. 221,828. U. K. P. Office, 1925
1930	Thermal spray companies founded	Metco/MONGUL/Metallisation	"ITSA History," International Thermal Spray Association, http://www.thermalspray.org/index.php?option=com_content&task=view&id=58&Itemid=92
1937	Colomony's spray and fuse	N.W. Cole.	N.W. Cole and W. H. Edmonds, "Hardening material resistant to heat, acid, corrosion, and abrasion, and method of producing the same." USA Patent No. 2088838. U. S. P. Office, 1937
1938	Flame spray/Type E torch	Metco	"History: Over 75 years of Sustainable Surface Solutions," Sulzer Metco, http://www.sulzer.com/en/About-us/Our-Businesses/Sulzer-Metco/History
1939	Plasma spray	Reinecke	J.R. Davis, *Handbook of Thermal Spray Technology,* ASM International, Materials Park, OH, USA, 2004
1950	ThermoSpray Powder Gun	Metco	"History: Over 75 years of Sustainable Surface Solutions," Sulzer Metco, http://www.sulzer.com/en/About-us/Our-Businesses/Sulzer-Metco/History
1955	D-Gun®	R.M. Poorman/Union Carbide	R.M. Poorman, H. B. Sargent, and L. Headlee, "Method and apparatus utilizing detonation waves for spraying and other purposes." USA Patent No. 2714563. U. S. P. Office, 1955
1957	Flame spray/Rokide® ceramic coating	Norton Company	C.W. Cheape, *Family Firm to Modern Multinational: Norton Company, A New England enterprise*, Harvard University Press, 1985
1957	Plasma spray/Argon plasma torch	R.M. Gage/Union Carbide	R.M. Gage, "Arc torch and process." United States of America Patent No. 2806124. U. S. P. Office, 1957
1960	Plasma spray/SG-1 torch	G.M. Giannini/Plasmadyne Corporation	G.M. Giannini and A.C. Ducati, "Plasma Stream Apparatus and Methods." USA Patent No. 2,922,869. U. S. P. Office, 1960
1967	RF Plasma	T.B. Reed/Massachusetts Institute of Technology	T.B. Reed, "Induction plasma torch with means for recirculating the plasma." United States of America Patent No. 3324334. U. S. P. Office, 1967
1960	Plasma spray/MB series torches	Metco Inc.	"History: Over 75 years of Sustainable Surface Solutions," Sulzer Metco, http://www.sulzer.com/en/About-us/Our-Businesses/Sulzer-Metco/History
1960	Twin wire arc/torch improvements	Various authors	D.M. Yenni, W.C. Mcgill, and J.W. Lyle, "Electric arc spraying." USA Patent No. 2982845. U. S. P. Office, 1961 G.A. Jensen, "Device for coating substrates." USA Patent No. 3140380. U. S. P. Office, 1964 I. Kiyoshi, "Method of and apparatus for the electric spray-coating of substrates." USA Patent No. 3358114. U. S. P. Office, 1967
1973	Plasma spray/LPPS	E. Muehlberger/Electro-Plasma Inc.	E. Muehlberger and P. Meyer, LPPS—Thin Film Processes: Overview of Origin and Future Possibilities, *Proceedings of the International Thermal Spray Conference 2009*, B.R. Marple, M.M. Hyland, Y.-C. Lau, C.-J. Li, R.S. Lima, and G. Montavon, Ed., 4-7 May 2009 (Las Vegas, NV, USA), ASM International, 2009, p 737-740.
1975	Plasma spray/SG100 torch	Plasmadyne Corporation	"Plasma Equipment Solutions," Praxair Surface Technologies Inc., Praxair Technology, Inc., USA, 2012
1979	Plasma spray/Gatorgard	L.S. Sokol/United Technologies Corporation	L.S. Sokol, C.C. McComas, and E.M. Hanna, "Plasma spray method and apparatus." USA Patent No. 4256779. U. S. P. Office, 1981.
1970	Plasma spray/F4 torch	Metco Inc.	"History: Over 75 years of Sustainable Surface Solutions," Sulzer Metco, http://www.sulzer.com/en/About-us/Our-Businesses/Sulzer-Metco/History
1982	HVOF/JetKote®	J.A. Browning	J. A. Browning, "Ignition method and system for internal burner type ultra-high velocity flame jet apparatus." USA Patent No. 4342551. U. S. P. Office, 1982
1988	Plasma spray/APG torch	Metco Inc.	"History: Over 75 years of Sustainable Surface Solutions," Sulzer Metco, http://www.sulzer.com/en/About-us/Our-Businesses/Sulzer-Metco/History

Table 1 continued

Year	Application	Lead inventor/Company	Reference details
1989	HVOF/second Generation	Various suppliers	F. Gärtner, H. Kreye and H. J. Richter, HVOF spraying with powder and wire, *7th Colloquium HVOF Spraying* C. Penszior and P. Heinrich, Ed., 9-10 November 2006, (Unterschleißheim, Germany), GTS e.V., 2006
1990	Super D-Gun®	Union Carbide Coatings Service Corporation	B. J. Gill, *Super D-Gun*, Aircraft Engineering and Aerospace Technology, 62, MCB UP Ltd., 1990, p 10-33
1980	Cold Spray	A. Papyrin	A. Papyrin, Cold spray technology. *Advanced Materials and Processes*, 2001, 159(9), p 49-51
1980	TWA/Equipment improvements	Various suppliers	L. Pawlowski, *The Science and Engineering of Thermal Spray Coatings*, Wiley, Chichester, 2008
1992	Plasma spray/PlazJet 170kW torch	Praxair	K. E. Schneider, V. Belashchenko, M. Dratwinski, S. Siegmann, and A. Zagorski, *Practical Experience Today*, Thermal Spraying for Power Generation Components, Wiley-VCH Verlag GmbH & Co. KGaA, 2006, p 17-104
1992	HVOF/third Generation	Various suppliers	F. Gärtner, H. Kreye, and H.J. Richter, HVOF spraying with powder and wire, *7th Colloquium HVOF Spraying* C. Penszior and P. Heinrich, Ed., 9-10 November 2006, (Unterschleißheim, Germany), GTS e.V., 2006
1992	RF Plasma/1 MW torch	M.I. Boulos/Tekna	M. I. Boulos and J. Jurewicz, "High performance induction plasma torch with a water-cooled ceramic confinement tube." USA Patent No. 5200595. U. S. P. Office, 1993
1990	Water-stabilized plasma spray	M. Hrabovský/Institute of Plasma Physics ASCR	M. Hrabovský, Water-stabilized plasma generators. *Pure and Applied Chemistry*, 1998, 70(6), p 1157-1162
1990	Plasma spray/Triplex 24kW torch	Sulzer Metco	"History: Over 75 years of Sustainable Surface Solutions," Sulzer Metco, http://www.sulzer.com/en/About-us/Our-Businesses/Sulzer-Metco/History
1994	Plasma spray/Axial III torch	Northwest Mettech Corp.	"About Us: Northwest Mettech," Northwest Mettech Corp, http://www.mettech.com/company/corporate/about-us.html.
1995	DPV 2000/Particle diagnostics	Tecnar Ltd.	"TECNAR Spray Diagnostics Products: Online Characterization Of Particles During Thermal /Cold Spraying," Tecnar Ltd., http://www.tecnar.com/index.php/products/spray-diagnostics
1998	Plasma spray/Triplex II 55kW torch	Sulzer Metco	"History: Over 75 years of Sustainable Surface Solutions," Sulzer Metco, http://www.sulzer.com/en/About-us/Our-Businesses/Sulzer-Metco/History
1998	Plasma-transferred wire arc spray	D.R. Marantz/Ford Global Technologies, Inc.	D.R. Marantz, K. A. Kowalsky, J. R. Baughman and D. J. Cook, "Plasma transferred wire arc thermal spray apparatus and method." USA Patent No. 5808270. U. S. P. Office, 1998
1999	SprayWatch/Particle diagnostics	Oseir Ltd.	"Company Info: Oseir Ltd.," Oseir Ltd., http://www.oseir.com/
2001	Plasma spray/100HE 105kW torch	Progressive Technologies	"Improving the Economics of Plasma Spray: 100HE Sixteen Hour Durability Run," Progressive Technologies, http://www.progressivesurface.com/downloads/casestudies/100HE_16hour_run.pdf, 2003.
2000	Cold Spray/Kinetics family torches	CGT GmbH.	"Linde launches cold spray technology," http://www.gasworld.com/linde-launches-cold-spray-technology/1702.article, 2007
2006	Warm Spray	J. Kawakita/NIMS	J. Kawakita, S. Kuroda, S. Krebs and H. Katanoda, In-situ densification of Ti coatings by the warm spray (two-stage HVOF) process. *Materials Transactions*, 2006, 47(7), p 1631-1637
2008	Nano-ceramic coatings	Northwest Mettech Corp.	J. Oberste Berghaus, J. G. Legoux, C. Moreau, R. Hui, C. Decès-Petit, W. Qu, S. Yick, Z. Wang, R. Maric and D. Ghosh, Suspension HVOF spraying of reduced temperature solid oxide fuel cell electrolytes, *Journal of Thermal Spray Technology*, 2008, 17(5-6), p 700-707
2009	Plasma spray/PlazJet II 220kW torch	Praxair TAFA	"Plasma Equipment Solutions," Praxair Surface Technologies Inc., Praxair Technology, Inc., USA, 2012

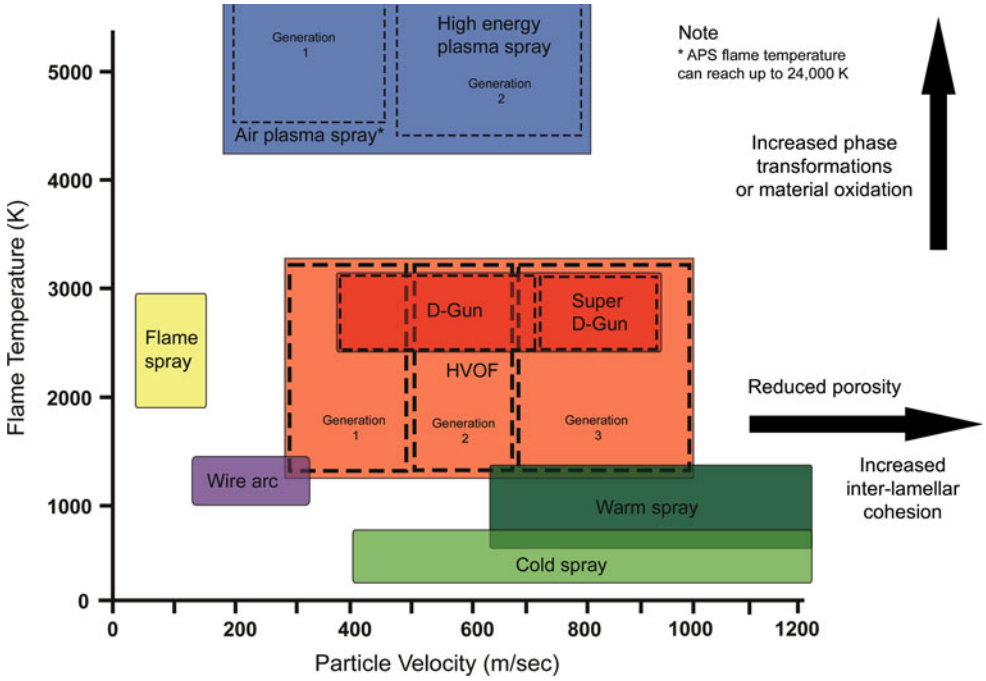

Fig. 2 Classification of thermal spray processes with accordance to particle velocity and flame temperature

Table 2 Comparison of typical process variables in thermal spray technology

Spray process	Flame temperature, K	Particle velocity, m/s	SOD, mm	Width of spray footprint, mm
FS	3000	150	120-250	50
TWA	6000	240	50-170	40
D-Gun®	4500	750	100	<25
APS	10000	350	60-130	20-40
LPPS	15000	600	300-400	50-60
HVOF	3400	650	150-300	<20
CS	1000	800	10-50	<5

Fig. 1 and 2 illustrate that advances in thermal spray technology are a direct consequence of altering the temperature-velocity characteristics of the spray devices. Therefore, the TS maps that will be presented later may be cross-indexed onto Fig. 2 so that a concordance approach evolves. The cross correlation of distribution analyses involving (i) the TV characteristics and (ii) the property-process relationships is beyond the scope of this review.

The third critical factor in thermal spray processing revolves around the feedstock. Depending on the thermal spray operation considered, an appropriate combination between the feedstock material and size must be considered. Table 3 compiles a list of commercially available powder feedstocks and the associated thermal spray method that is typically employed (Ref 13–16). Correct selection of feedstock is critical since this decision relates to the deposition efficiency of the process and, therefore, the overall manufacturing economics.

3. Material Genomic Approach for Thermal Spray

Although thermal coatings have been produced for certain applications, there are certain material properties that are mutually dependent. These properties include (i) porosity, (ii) hardness, (iii) adhesion, (iv) elastic modulus, (v) fracture toughness, and (vi) the Poisson's ratio of thermal spray coatings. A scoping study for relevant data from the literature revealed that this was a complex task. For example, it was necessary to consolidate and standardize the property data of different coatings that had been manufactured with a variety of equipment under diverse reporting standards.

The issue of reporting standards and lapses in documentation in the open literature focussed the current study toward classes of materials and processes that can be considered of widespread popularity. For instance, WC-Co coatings are extensively used as wear-resistant

Table 3 Compilation of commercially available powders produced via the various production methods

Classification	Material constituents	Possible production method								Application method
		Gas atomized	Water atomized	Fused and crushed	Sintered and crushed	Agglomerated and sintered	Dense coated	Plasma densified	Blend	
Metal/metallic alloy	Al, Al-Si	X								APS, CS, FS
	Cu, Cu-Ni, Cu-Al	X								HVOF, APS, CS, FS
	Ti, Ta	X								VPS, CS
	FeCr, FeCrNiMo, FeCr based	X	X				X			APS, FS
	MCrAlY (M=Co, Ni, Fe)	X								APS, HVOF,VPS
	Mo, Mo based				X	X		X		APS
	Ni, Ni-Cr, Ni-Al, Ni based,	X	X				X			APS, FS, CS, HVOF, VPS
Metallic composite	Al-Si-based abradables						X		X	APS, FS
	CoNi-based abradables								X	APS
	Ni-based abradables						X			FS
	Cu-Al-Bronze						X			HVOF, APS
Intermetallic	CoCrNiWC, CoCr based	X	X							HVOF, APS
	NiCrSiB, NiCrSiB-based, self-fluxing alloys	X	X							FS, HVOF
Cermet	Mo-Mo_2C					X				APS
	CrC-NiCr, CrC-Ni based				X	X	X		X	APS HVOF FS
	WC-Co, WC-Ni, WC based				X	X	X	X		APS HVOF FS
Ceramic	Al_2O_3, Al_2O_3- TiO_2			X					X	APS, FS
	Cr_2O_3, Cr_2O_3-TiO_2, Cr_2O_3-TiO_2-SiO_2			X	X	X			X	APS
	TiO_2			X						APS, FS
	ZrO_2-Y_2O_3, ZrO_2-MgO			X		X		X		APS

FS: Flame spray. APS: Atmospheric plasma spray. VPS: Vacuum plasma spray. HVOF: High-velocity oxygen fuel spray. CS: cold spray

coatings and alumina-based coatings represent a large proportion of the market for thermal spray as anti-wear and corrosion-resistant coatings. Although there is an emphasis on these materials, it can be pointed out that they can be sprayed by many processes, the maps of which are very informative as will be presented later.

The material-property measurements of thermal spray coatings are related to the lamellar microstructure. Analyzing the literature on thermal spray coatings is challenging due to the many types of feedstock, spray systems, spray parameters, and other variables that influence the coating final structure. The lack of an overall framework for the presentation of properties has also arisen because researchers have focused on the properties and performance of specific coatings or processes rather than relationships among the entire family.

Relationships among the feedstock materials, thermal spray methods, and spray parameters have been drawn by compiling the mechanical properties into a single database. This material genomic approach is depicted in a flow chart, Fig. 3. The database structure was constructed and then populated by reviewing the available literature so that trends could be discerned. In this manner, the broader relationships of thermal spray coatings were explored by constructing plots that summarized data to show the interactions between processes and materials. These so-determined scatter plots were inspired, in part, by the material selection plots formulated by Prof. M. Ashby of Cambridge University in the United Kingdom (Ref 10). The Ashby scatter plots displayed two or more properties of many materials or classes of materials. Similarly, the "thermal spray property-performance maps" (termed as "TS maps") created in the current work have incubated a fresh perspective that has allowed a balanced comparison of results across different laboratories.

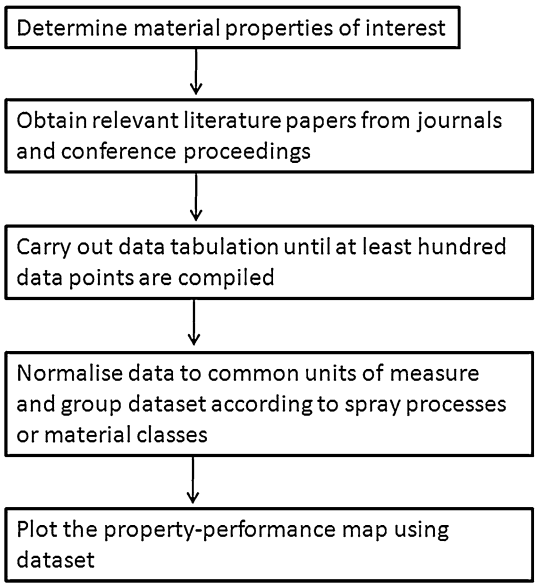

Fig. 3 Flow chart to describe TS PPM construction process

It must be noted that the TS maps are conceptually different from process maps in thermal spray technology (Ref 17, 18) which are used to assess coating reliability. Process maps have been yielded from the in situ monitoring of the temperature and velocity spray profile of the powder particles and splats. These process maps are constructed on the basis of experimental work and are specific for a defined feedstock. Hence, it can be recognized that TS maps provide an overview of the different processes and feedstocks available, while "process maps" relate specifically to the variability in a particular spray-feedstock system.

The following section compiled test data of commonly investigated thermal spray coating properties from the published literature. There is a natural, intrinsic cause and effect relationship among the temperature-velocity conditions, the feedstock materials, and their particle size distribution. Thus, analysis of these datasets was expected to yield observable trends and comparisons with regard to the thermal spray processes. Such a retrospective analysis and review has not been reported previously.

4. Review of Thermal Spray Coating Property Data

Five frequently investigated coating properties will be presented in this work. The TS maps are focussed on porosity, hardness, coating adhesion, elastic modulus, and sliding wear performance of thermal spray coatings. It is important to emphasize that this study was intended as a broad survey of coating properties. All of the experimental details are presented in the original manuscripts and the properties determined by these original investigators were applied to studies within their own context.

The first step to construct TS maps was to assemble data from the literature and standardize the units of measure. The complexity of data collection laid in dealing with the different reporting formats and in some cases interpreting and estimating the reported values. These data were then plotted onto scatter graphs with common axes.

The TS maps presented in this study were plotted from approximately 100 individual data points. Figure 3 is a flow chart that describes the TS map construction procedure. Six TS maps are reviewed in this study and these can be considered as typical of the information that can be revealed by careful analysis.

4.1 Map 1: Hardness-Porosity of Thermal Sprayed WC-Co Coatings

The scatter plot of hardness and porosity of tungsten carbide-cobalt (WC-Co) composite coatings is presented in Fig. 4. Four thermal spray methods are represented in the plot: atmospheric plasma spray (APS), high-velocity oxygen fuel (HVOF) spray, detonation gun (D-Gun®) spray, and cold spray (CS). These deposition techniques are typically used for WC-Co coatings. The units of hardness have

been normalized to GPa and only cross-sectional microhardness test values considered. The differences in the test method, i.e., Vickers and Knoop tests, have been assumed to be negligible. The authors appreciate that these hardness techniques sample different volumes of materials under dissimilar stress conditions; however, pooling such data allows a more comprehensive database to be created without compromising data quality to a large degree. The coating porosity data can be quantified by many methods (Ref 19, 20) and the data across techniques are presumed indifferent for the purposes of this current study.

The assumptions stated above can be disputed. However, this current study is aimed at setting a foundation for future data-mining exercises where limitations that depend on reporting and testing protocols can be more rigorously resolved. In other words, one of the outcomes of this review is that all investigators need to report testing methods and protocols more meticulously so that data-mining exercises may be prescribed in the future.

Figure 4 reveals a large degree of variance of coating hardness across the four spray methods. A clustering of data points for each individual spray method can be identified. Thermal spray techniques, such as CS and D-Gun®, which use high particle kinetic energy for coating formation, lead to a low coating porosity and high coating hardness. The high thermal input of APS coating deposition produced coatings with large numerical variations in porosity and hardness. The thermal spray footprint, or spray envelope, of the APS process is significantly larger and more flat than those of HVOF, D-gun®, and CS, refer to Table 2 and Fig. 2. Thus, the TV processing zone is more variable and this leads to material characteristics that are highly dispersed. It can also be observed for the HVOF and D-gun® processes, where there are statistically significant data, that low porosity materials revealed hardness data that were clustered. That is, processes that lead to high-density coatings will also give rise to the most reliable material characteristics.

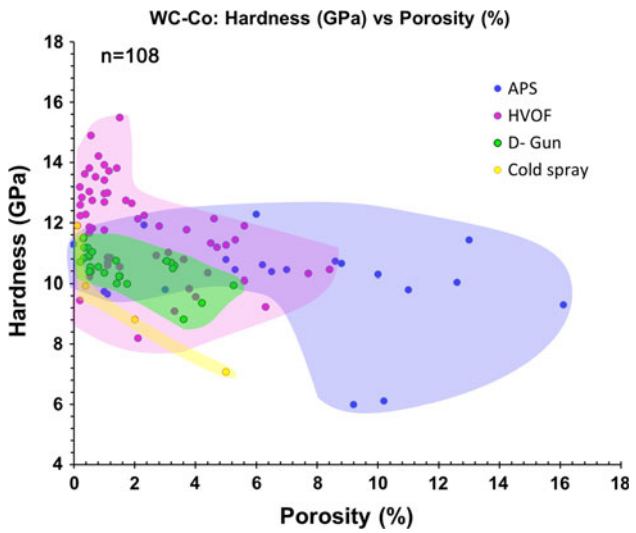

Fig. 4 Hardness-porosity map of thermal spray tungsten carbide-cobalt coatings ($n = 108$ data points)

The APS process also leads to decarburization of WC to W_2C, which can occur at high temperature. This phase transformation creates formation of a brittle phase that increased the overall coating hardness (Ref 21) and which has contributed to the data scatter. Another reason for the data scatter arose due to differences in feedstock and spray parameters. For instance, there can be changes in the coating composition between the ratio of ceramic WC and metallic cobalt feedstock. Different laboratory or research groups may also choose to experiment with (i) a unique blend of WC-Co, (ii) different feedstock size, or (iii) spray parameters.

Nevertheless, the general trend is that the microstructural porosity decreases with increasing coating hardness. In other words, a dense coating would have a higher coating hardness compared to a porous coating. Although this conclusion might be as expected on the basis of a fundamental understanding of material-property relationships, the TS map allows visualization of (i) relationships among different TS processes, (ii) a broad ranking of the TS processes with respect to porosity and hardness, (iii) aim values for specific hardness and porosity combinations, and (iv) the reliability of obtaining specific properties on the basis of process reproducibility.

4.2 Map 2: Hardness-Porosity of Thermal Sprayed Alumina Coatings

Alumina (Al_2O_3) and alumina-based (i.e., Al_2O_3-TiO_2) coatings have significant industrial applications and, thus, these coatings have been data mined in greater detail. The TS map for alumina is plotted using the same methods and assumptions from the WC-Co map. In addition to the four earlier mentioned thermal spray techniques, other methods such as low pressure plasma spray (LPPS), solution precursor plasma spray (SPPS), and high-velocity suspension fuel spray (HVSFS) have been included on the map. Eight thermal spray processes are represented in Fig. 5.

It can be noted that the common spray techniques were identifiable by highlighted clusters. Pure alumina coatings exhibited higher hardness; however, the coatings were also brittle. Thus, 2 to 4 wt% of titania is usually blended with the alumina feedstock to increase the toughness of the thermal spray coating. Coatings produced from materials with increasingly higher percentages of titania, commonly 13 or 40 wt.% TiO_2, exhibited lower hardness (Ref 22, 23). Coatings produced via CS must include a metallic binder that would have lowered the average hardness values.

Alumina also exhibited several phases, the most stable being the alpha phase. Almost all sintered alumina products are available in the hexagonal close-packed structures of the alpha phase. On the other hand, due to the rapid melting and quenching rates of thermal spray processes, gamma phase alumina was prevalent within a thermal spray coating (Ref 24, 25). The gamma phase is a fine-grained alumina that exhibits the cubic spinel structure. In the case of thermal spray alumina coatings, the phase

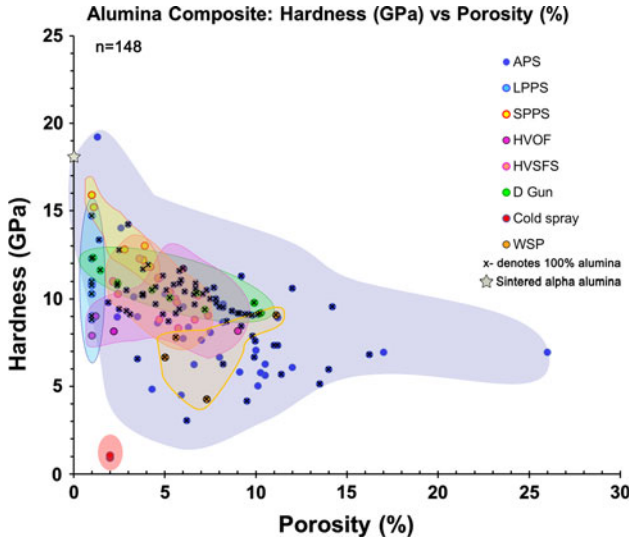

Fig. 5 Hardness-porosity map of thermal spray alumina composite coatings ($n = 148$ data points). Note: "x" overlay symbol represents pure alumina coatings

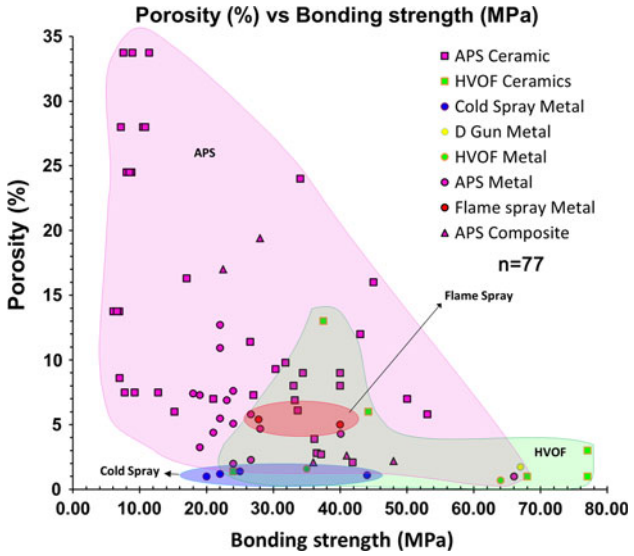

Fig. 6 Porosity-bond strength map of thermal spray coatings from different processes ($n = 77$ data points). The coating classes are distinguishable by the plot shape; metallic coatings are plotted as circles, ceramic coatings are plotted as squares, and composites are shaped as triangles

changes did not influence the hardness values as markedly as the decarburization of WC-Co phase. Gamma alumina has a lower hardness compared to the alpha phase that exhibits a hardness of approximately 16-20 GPa. It can be seen from the microhardness axis of Fig. 5 that, due to the presence of gamma alumina within the spray coating microstructure, coating hardness is lower than for sintered alpha alumina ceramics.

It should be noted that some of the compiled data consisted of thermal spray coatings that were heat treated. The gamma phase converts to the alpha phase at sintering temperatures above 1000 °C (Ref 24, 26). These heat-treated coatings exhibited increased hardness and reduced porosity due to grain coarsening. By comparison, the gamma structure exhibited a higher specific surface area compared to the alpha phase. Therefore, during transformation from gamma to alpha alumina, densification of the coating microstructure occurred (Ref 24).

The general trend within Fig. 5 is similar to the previous TS map; hardness decreases with increasing coating porosity. Coatings with near to zero porosity can be achieved with thermal spray processes such as the LPPS, SPPS, and HVSFS. Although, not displayed in Fig. 2, SPPS and HVSFS are emerging thermal spray methods that allow the deposition of nanostructured alumina coatings using a liquid-based feedstock. APS offered the most flexible thermal spray process to achieve coatings with a wide-ranging porosity level.

4.3 Map 3: Porosity-Bond Strength of Thermal Spray Coating

The two TS hardness-porosity maps presented previously establish the trend that hardness decreases with increasing porosity. The next TS map explores the effects of coating porosity on bond strength. Collation of tensile adhesion test data (TAT) of thermal spray coatings performed using the ASTM C633 standard (Ref 27) or its equivalent was carried out. The reported TAT data have been normalized to MPa by taking the ratio of the failure load to the test area of the coating. In cases when a range of values for a particular coating system was quoted within the research work, an average value was calculated. The corresponding porosity levels were also gathered and plotted collectively to form the porosity-bond strength TS map seen in Fig. 6.

Five thermal spray processes are represented in the TS map and have been outlined by different color shades. The graph legend displays the different combinations of process and materials' classes. The thermal spray processes are APS (pink), HVOF (green), CS (blue), flame spray (red), and D-Gun® (yellow). Coating details such as feedstock type and spray parameters have not been included within this TS map to maintain clarity. Although this generalization simplifies the scatter plot for user interpretation, there is a loss of information such as the mode of failure for individual data points. In addition, the original data points have not been classified with regard to experiment conditions such as the type of adhesive, the specimen geometry, or coating thickness. As mentioned earlier, each data point has been treated as unique information since the original authors were seeking specific data for their own study.

It can be ascertained from the scatter plot that bond strength increased with decreasing porosity. The TS map also affirms that thermal spray deposition methods such as HVOF and D-Gun® were associated with coatings of high bond strength and low porosity. The APS method revealed a large variance on measured bond strength that probably depended on the coating application. Coatings for biomedical applications (i.e., hydroxyapatite) and

thermal barrier protection (i.e., yttria-stabilized zirconia) required intentional porosity within the microstructure. The APS method offered the most flexible deposition option in these instances. However, the large void content acted as stress concentrators or failure sites for crack growth and gave rise to low bond strength (Ref 28).

4.4 Map 4: Hardness-Bond Strength of Thermal Spray Coating

The relationship of coating bond strength among material classes was investigated on a TS map that was based on coating hardness. The reasoning was that thermal spray ceramic coatings would present higher coating hardness values than metallic ones. The fourth TS map is, therefore, presented in Fig. 7 and exhibits the microhardness vs. bond strength for several thermal spray coatings. The three classes of material are color shaded: ceramics (red), metals (green), and composites (yellow).

Figure 7 indicates that metallic thermal spray coatings exhibited greater bond strengths than ceramic coatings. Coated ceramics revealed high microhardness, but relatively more data points of low tensile bond strength. Metallic coatings have high bond strength, but low microhardness values. The minimum failure stress was also comparatively higher for metallic thermal spray coatings. The reasons for the difference in bond strengths are probably related to the effective intersplat contact, coating residual stress, and failure mechanism (Ref 29, 30). These factors are not reflected in this particular TS map and insufficient data exist to document additional TS maps.

The failure strength of thermal spray composite coatings, for example, WC-Co, exhibited properties that overlapped its parent material classes, i.e., metals and ceramics, and the properties depended on the relative coating composition and spray method. Within the same material class, the HVOF and VPS methods exhibited the highest bond strength, which was associated with their dense coating microstructure.

4.5 Map 5: Porosity-Elastic Modulus of Thermal Spray Coating

The consolidation of the elastic modulus data for thermal spray coatings would reveal any dissimilarity in this mechanical property compared to bulk materials. The elastic moduli for common bulk engineering materials were compiled from references (Ref 31, 32), Table 4. The differences arise due to the unique microstructure of a thermal spray coating since they exhibit intersplat, pseudo-ductile behavior. There are many methods, as well as several prime specimen orientation directions, to measure coating elastic modulus, all of which make data normalization challenging. Firstly, both tension and compression testing data are considered, with the majority of available data reported in the compression mode.

Table 4 The bulk elastic modulus properties of common engineering materials

	Material	Elastic modulus (*E*), GPa
Metals	Al	67
	Cu	128
	Fe	208
	Zn	69-138
	Ni	207
	Ti	120
Ceramics	TiO_2 (rutile)	283
	Al_2O_3 (alpha)	380
	Cr_2O_3	>103
	Partially stabilized ZrO_2	205
	Fully stabilized ZrO_2 (cubic)	97-207
	Cr_3C_2	373
	Cemented carbides	96-654

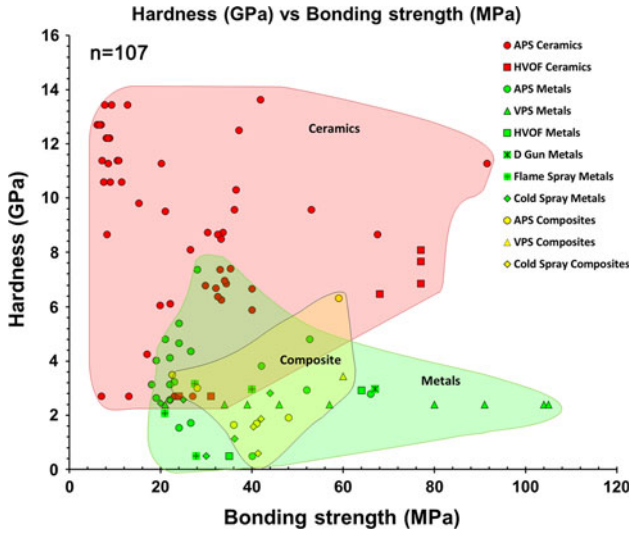

Fig. 7 Hardness-bond strength map of thermal spray coatings from different material classes ($n = 107$ data points). The shape of the data points represents the spray technique

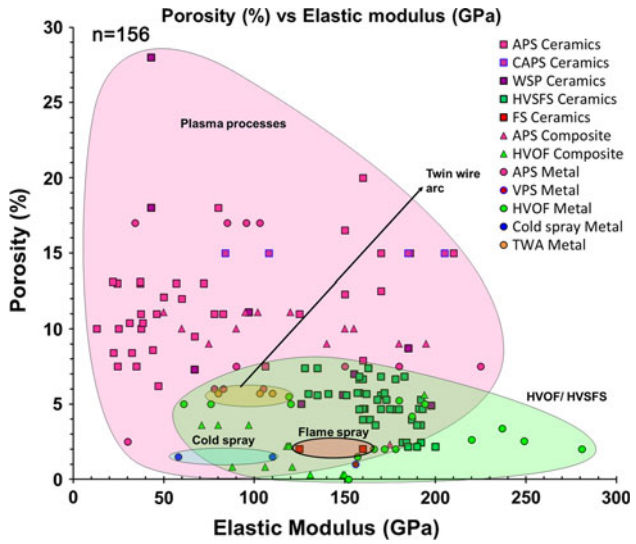

Fig. 8 Porosity-elastic modulus map of thermal spray coatings from different processes ($n = 156$ data points)

In addition, the porosity-elastic modulus data consist of both in-plane and cross-sectional elastic modulus for thermal spray coatings. All of the available data are presented for completeness so that appropriate comparisons to the bulk material can evolve, although it has been mentioned earlier that the coating elastic moduli are interrelated with specimen orientation. Finally, the units for elastic modulus were standardized to GPa. Therefore, after data normalization, the fifth TS map is presented in Fig. 8. The style of the plot is consistent with the earlier TS maps; that is, the five individual thermal spray processes are color shaded and the legend indicates the three different material classes.

Two observations can be made concerning the range of coating elastic moduli. Firstly, the values for ceramic thermal spray coatings were significantly lower than for the corresponding bulk sintered ceramic values. In-plane coating elastic modulus was expected to be higher than the cross-sectional values due to the anisotropic lamellar microstructure that offers limited pseudo-ductility in that direction. However, from Fig. 8, it is evident that a majority of the thermal spray ceramic coatings (square-shaped data) do not exceed an elastic modulus of 200 GPa. For instance, some values of sintered ceramics (Ref 33) are as follows: alumina is 380 GPa; titania is 283 GPa; and partially stabilized zirconia is 205 GPa. Therefore, the effects of intersplat sliding within the porous microstructure of the coating reduced the effective stiffness. In other words, the stiffness values of thermal spray ceramic coatings will be significantly lower compared to bulk ceramics, especially in instances where coating porosity increases.

The second observation relates to the higher values of elastic modulus for metal thermal spray coatings, depicted as circles in Fig. 8. This unexpected effect arose probably due to the oxidation of metallic splats during the thermal spray process. The formation and entrapment of metal oxides within the coating microstructure would have caused an increase in the overall coating modulus.

Figure 8 demonstrates that thermal spray coatings deviate considerably from the conventional elastic properties of the corresponding bulk material. The general trend exhibited is that the coating elastic modulus decreased with increasing porosity. A physical interpretation is that there would be a greater tendency of lamellae sliding due to regions of poor intersplat contact (Ref 34, 35). Plasma-based thermal spray processes revealed the largest data variation among the spray methods. The properties depended on the porosity levels as well as phase transformations that occurred during the spray process. High kinetic energy spray processes, such as HVOF, HVSFS, and CS techniques, exhibited less scatter in these data since the porosity levels were low and the coating properties would be affected only by phase transformations.

4.6 Map 6: Hardness-Elastic Modulus of Thermal Spray Coating

It would be expected that the elastic modulus of ceramics be greater than that of metals. Therefore, using the same concept as in TS Map 4, coating hardness data were used to discriminate the various material classes. The coating elastic modulus was plotted against the microhardness data to determine whether the expected trend could be validated. The three types of material classifications were identified by the same color scheme adopted for TS Map 4. The results, Fig. 9, show that metal coatings appear on the lower region compared to ceramic coatings, which is consistent with fundamental material-property behavior.

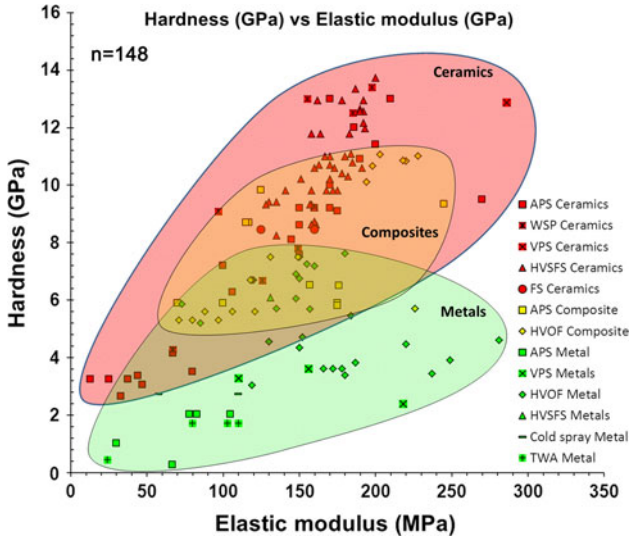

Fig. 9 Hardness-elastic modulus map of thermal spray coatings from different processes ($n = 148$ data points)

The general trend is that the elastic modulus increases with coating microhardness, which follows the expected trend that modulus and hardness are positively correlated. It must be noted that only the corresponding cross-sectional elastic moduli values of coatings were taken into consideration to be consistent with the coating cross-sectional microhardness values.

Plasma-based processes are widely used methods for deposition of ceramic coatings, whereas HVOF techniques are more common for metal-based coatings. Both methods are able to produce the greatest coating elastic modulus and hardness readings among their respective material class.

The six property-performance TS maps constructed in this work allow a systematic analysis for the material properties of thermal spray coatings with respect to thermal spray processes. The scatter plots consisted of more than 80 data points across many variants of deposition techniques and feedstocks from different researchers and laboratories. The nature in which these data were collected involved an unbiased representation so that no specific research group or publication paper could be favored.

The new approach taken in this work is more significant than a conventional literature review. The property-performance TS maps have indicated an ability to interrelate all data within the field of thermal spray and provide a

holistic explanation to coating properties. The TS map approach was different from that of TS processing map methods, which suggested that particle velocity and flame temperature play a critical role in coating microstructure as depicted in Fig. 2.

The TS processing map proposition is that increasing particle velocity, such as conferred by high kinetic energy processes, decreased the porosity and increased the intersplat cohesion. There was increased thermal phase transformation for high thermal input processes. The effects of porosity, intersplat cohesion, and thermal phase transformation are all represented within the trends of the TS maps in this study.

A summary of the trends and TS map details is presented in Table 5. Thus, TS maps lend unbiased and strong evidence to suggest that combinations of spray processes, spray parameter tables, and feedstocks yield variations to the coating properties in a systematic and ordered fashion.

4.7 Other Possible TS Mapping Techniques/ Combinations

A similar data-consolidating procedure can be employed to map out the application-specific performance of thermal spray coatings and provide an overview of

Table 5 Summary of TS map trends and details

Map number	Trend	Number of data points	Year earliest reference	Year latest reference
1: Hardness-porosity (WC-Co)	Porosity decreases with increasing coating hardness	108	1997	2010
2: Hardness-porosity (alumina)	Porosity decreases with increasing coating hardness	148	1997	2010
3: Porosity-bond strength	Bond strength increases with decreasing porosity	77	2001	2011
4: Hardness-bond strength	Metal-based thermal spray coatings show better bond strengths than their ceramics counterparts	107	2001	2011
5: Porosity-elastic modulus	Coating elastic modulus decreases as porosity increases	156	1997	2010
6: Hardness-elastic modulus	Elastic moduli of ceramics coatings are greater than that of metallic coatings. Increasing microhardness with increases in the elastic modulus	148	1997	2010

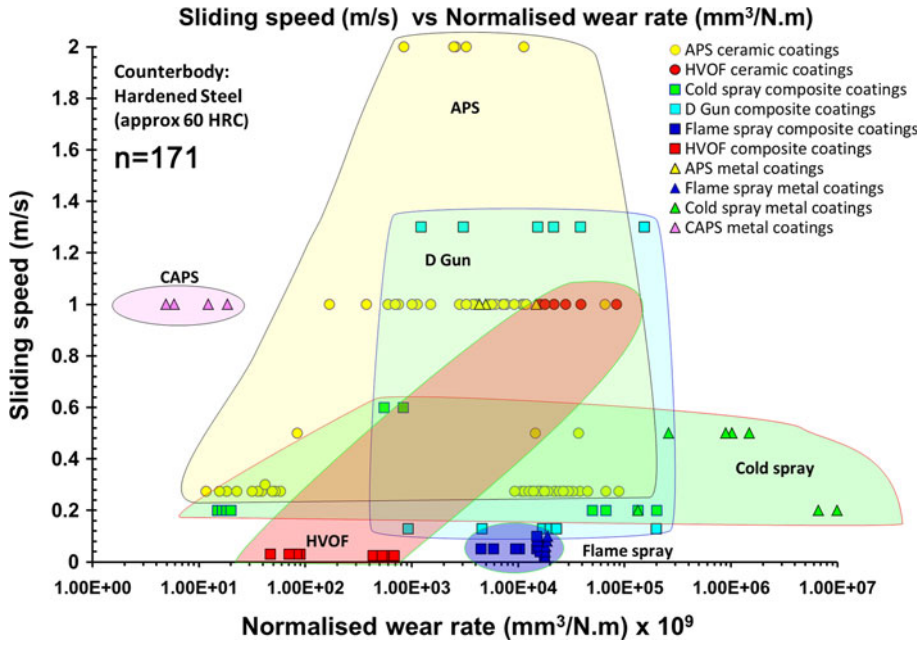

Fig. 10 Sliding wear rate of various thermal spray coating plotted against sliding speed ($n = 171$ data points)

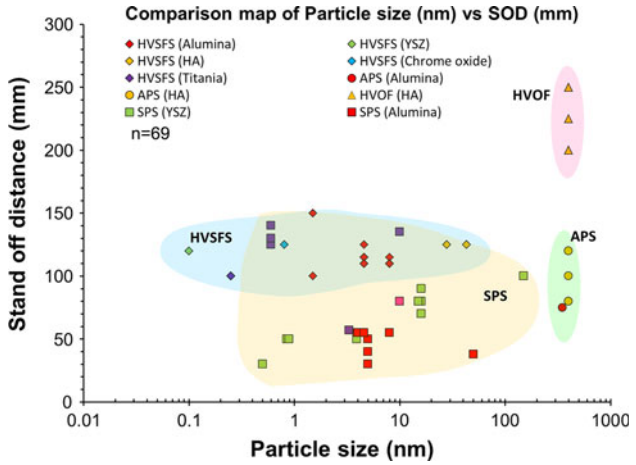

Fig. 11 Map to suggest required standoff distance for various starting feedstock sizes ($n = 69$ data points)

potential coating solutions. An example of a wear application map is presented in Fig. 10. It must be pointed out that this wear application map is compiled based on reported experiments and shows wear rate at a specific sliding speed, which depended on the researcher. This map also reveals the conundrum with sliding wear testing for thermal spray materials, i.e., there were no standardized test speeds. Figure 10 highlights this gap in knowledge. Also, this map indicates that APS ceramic coatings should be a possible solution for applications that require high sliding speeds.

Alternatively, process evaluation TS maps can be constructed. Figure 11, for example, provides an estimate of the required standoff distance for different feedstock sizes. This TS map provides a useful teaching tool to explain the fundamental relationships between feedstock and standoff distance with regard to the need for different spray distances for different processes. It can be said that as the particle size decreases for each of the thermal spray families (i.e., plasma or combustion energy source), the standoff distance also decreases.

Hence, such TS maps can be a tool to aid the design of a new generation of thermal spray coatings by highlighting existing gaps and frontiers in the current technology.

5. Conclusions

Thermal spray coatings are identified by a lamellar microstructure formed from the rapid solidification of molten droplets and cohesion among splats. This structure gave rise to the anisotropic mechanical behavior of coatings produced via different thermal spray methods since a distinctive splat structure and associated void system was created.

A comprehensive literature survey was conducted to compile relevant thermal spray coating property vs. performance data. The six property-performance TS maps constructed in this work showed the ability to interrelate all data within the field of thermal spray and provided a holistic explanation to coating properties. TS maps have been created with respect to porosity, hardness, coating adhesion, and elastic modulus. The effects of porosity, intersplat cohesion, and thermal phase transformation are all represented within the trends of the TS maps. This understanding agreed with the notion that particle velocity and flame temperature play a critical role in creating the coating microstructure.

Acknowledgments

This work was supported under a Swinburne University Postgraduate Research Award. We also acknowledge support from the Defence Materials Technology Centre (DMTC).

References

1. J.R. Davis, *Handbook of Thermal Spray Technology*, ASM International, Materials Park, OH, 2004
2. L. Pawlowski, *The Science and Engineering of Thermal Spray Coatings*, Wiley, Chichester, 2008
3. R. McPherson, The Relationship Between the Mechanism of Formation, Microstructure and Properties of Plasma-Sprayed Coatings, *Thin Solid Films*, 1981, **83**(3), p 297-310
4. S. Fantassi, M. Vardelle, A. Vardelle, and P. Fauchais, Influence of the Velocity of Plasma-Sprayed Particles on Splat Formation, *J. Therm. Spray Technol.*, 1993, **2**(4), p 379-384
5. M. Vardelle, A. Vardelle, and P. Fauchais, Spray Parameters and Particle Behavior Relationships During Plasma Spraying, *J. Therm. Spray Technol.*, 1993, **2**(1), p 79-91
6. P. Fauchais and G. Montavon, Plasma Spraying: From Plasma Generation to Coating Structure, *Advances in Heat Transfer*, vol. 40, Elsevier, Amsterdam, 2007, p 205-344
7. M.U. Schoop, An Improved Process of Applying Deposits of Metal or Metallic Compounds to Surfaces, U.K. Patent A.D. 21066, U. K. P. Office, 1912
8. Z.-K. Liu, and D.L. McDowell, Center for Computational Materials Design (CCMD) and Its Education Vision, *Materials Science and Technology (MS&T) 2006: Fundamentals and Characterization*, B. Fahrenholtz, A. Kimel, and P.E. Cantonwine, Eds., Cincinnati, OH, 2006, p 111-118
9. G.B. Olson, Computational Design of Hierarchically Structured Materials, *Science*, 1997, **277**(5330), p 1237-1242
10. M.F. Ashby, Chapter 4—Material Property Charts, *Materials Selection in Mechanical Design*, 4th ed., Butterworth-Heinemann, Oxford, 2011, p 57-96
11. S. Saber-Samandari and C.C. Berndt, IFTHSE Global 21: Heat Treatment and Surface Engineering in the Twenty-First Century: Part 10—Thermal Spray Coatings: A Technology Review, *Int. Heat Treat. Surf. Eng.*, 2010, **4**(1), p 7-13
12. A. Papyrin, Cold Spray Technology, *Adv. Mater. Process.*, 2001, **159**(9), p 49-51
13. Sulzer Metco, *Thermal Spray Materials Guide*, Sulzer Metco (US) Inc., Westbury, NY, 2012
14. Praxair Surface Technologies Inc., *Powder Solution Catalog: Praxair and TAFA Thermal Spray Powders*, Praxair Technology, Inc., USA, 2009
15. Amperit® Thermal Spray Powders, *Surface Technology*, H.C. Starck, Ed., H.C. Starck GmbH, Goslar, 2010
16. Flame Spray Technologies b.v., *Flame Spray Technologies: Powders*, Flame Spray Technologies b.v., Netherlands, 2008
17. M. Friis and C. Persson, Control of Thermal Spray Processes by Means of Process Maps and Process Windows, *J. Therm. Spray Technol.*, 2003, **12**(1), p 44-52

18. G. Dwivedi, T. Wentz, S. Sampath, and T. Nakamura, Assessing Process and Coating Reliability Through Monitoring of Process and Design Relevant Coating Properties, *J. Therm. Spray Technol.*, 2010, **19**(4), p 695-712
19. J. Ilavsky, G.G. Long, A.J. Allen, H. Herman, and C.C. Berndt, Use of Small-Angle Neutron Scattering for the Characterization of Anisotropic Structures Produced by Thermal Spraying, *Ceramics—Silikaty*, 1998, **42**(3), p 81-89
20. J. Matějíček, B. Kolman, J. Dubský, K. Neufuss, N. Hopkins, and J. Zwick, Alternative Methods for Determination of Composition and Porosity in Abradable Materials, *Mater. Charact.*, 2006, **57**(1), p 17-29
21. H.L. De Villiers Lovelock, Powder/Processing/Structure Relationships in WC-Co Thermal Spray Coatings: A Review of the Published Literature, *J. Therm. Spray Technol.*, 1998, **7**(3), p 357-373
22. A.A. Abdel-Samad, A.M.M. El-Bahloul, E. Lugscheider, and S.A. Rassoul, Comparative Study on Thermally Sprayed Alumina Based Ceramic Coatings, *J. Mater. Sci.*, 2000, **35**(12), p 3127-3130
23. M. Wang and L.L. Shaw, Effects of the Powder Manufacturing Method on Microstructure and Wear Performance of Plasma Sprayed Alumina-Titania Coatings, *Surf. Coat. Technol.*, 2007, **202**(1), p 34-44
24. R. McPherson, On the Formation of Thermally Sprayed Alumina Coatings, *J. Mater. Sci.*, 1980, **15**(12), p 3141-3149
25. P. Chráska, J. Dubsky, K. Neufuss, and J. Písacka, Alumina-Base Plasma-Sprayed Materials Part I: Phase Stability of Alumina and Alumina-Chromia, *J. Therm. Spray Technol.*, 1997, **6**(3), p 320-326
26. J. Ilavsky, C.C. Berndt, H. Herman, P. Chraska, and J. Dubsky, Alumina-Base Plasma-Sprayed Materials—Part II: Phase Transformations in Aluminas, *J. Therm. Spray Technol.*, 1997, **6**(4), p 439-444
27. ASTM C633-01(2008), *Standard Test Method for Adhesion or Cohesion Strength of Thermal Spray Coatings*, ASTM International, West Conshohocken, PA, 2008
28. K.A. Khor, C.S. Yip, and P. Cheang, Ti-6Al-4V/Hydroxyapatite Composite Coatings Prepared by Thermal Spray Techniques, *J. Therm. Spray Technol.*, 1997, **6**(1), p 109-115
29. R.C. Tucker, Jr., Structure Property Relationships in Deposits Produced by Plasma Spray and Detonation Gun Techniques, *J. Vac. Sci. Technol.*, 1974, **11**(4), p 725-734
30. H.D. Steffens, B. Wielage, and J. Drozak, Interface Phenomena and Bonding Mechanism of Thermally-Sprayed Metal and Ceramic Composites, *Surf. Coat. Technol.*, 1991, **45**(1-3), p 299-308
31. H. Baker, Properties of Metals, *Metals Handbook*, J.R. Davis, Ed., ASM International, Materials Park, OH, 1998
32. R.L. Lehman, Overview of Ceramic Design and Process Engineering, *Engineered Materials Handbook, 4, Ceramics and Glasses*, ASM International, Materials Park, OH, 1991, p 30
33. A.F. Liu, *Mechanics and Mechanisms of Fracture: An Introduction*, ASM International, Materials Park, OH, 2005
34. C. Li, A. Ohmori, and R. McPherson, The Relationship Between Microstructure and Young's Modulus of Thermally Sprayed Ceramic Coatings, *J. Mater. Sci.*, 1997, **32**(4), p 997-1004
35. S.H. Leigh, C.K. Lin, and C.C. Berndt, Elastic Response of Thermal Spray Deposits Under Indentation Tests, *J. Am. Ceram. Soc.*, 1997, **80**(8), p 2093-2099